

Realizable Unified RANS-LES and Dynamic LES Methods for Turbulent Flow Simulations

Stefan Heinz *

University of Wyoming, Laramie, WY 82071

Existing LES methods face three basic problems: a huge variety of LES models are currently applied, dynamic LES methods are either very expensive or have to be combined with flow-dependent empirical stabilization techniques, and the cost of LES for wall-bounded flow simulations are way too high for most applications. Solutions for these three problems can be developed by deriving non-dynamic, dynamic, and unified LES methods on the basis of a consistent stochastic theory. This approach results in a hierarchy of realizable LES models, corresponding dynamic LES methods that overcome the stability problems of existing dynamic LES methods, and unified RANS-LES methods that provide a reduction of LES cost by a factor of $0.07 Re^{0.46}$, which is huge for a high Reynolds number Re . The paper explains the theoretical background of the novel dynamic and unified LES methods based on stochastic analysis. Applications to several flows reveal the significant advantages of these methods in comparison to usually applied LES methods.

I. Introduction

The use of large eddy simulation (LES) is seen to represent the most promising way for developing a general and accurate computational method for the prediction of turbulent flows. However, experience with using LES reveals three basic problems:

- P1: Choice of SGS stress model: Previously, many models for the subgrid-scale (SGS) stress tensor have been designed to close LES equations.^{1,2} There are more than ten SGS model families available involving a variety of model options. Comparisons of all the models regarding a variety of flow simulations have never been performed. It is also questionable of how helpful such comparisons would be: there are no indications that one specific model performs much better than other models for a variety of flows. Usually, different models have advantages under certain conditions, making the choice of the SGS stress model difficult for a given condition.
- P2: Stability of Dynamic LES: The dynamic calculation of coefficients in SGS stress models is very attractive, but the success of such dynamic methods was limited so far. Germano's dynamic closure³ yields large fluctuations of model coefficients and results often in computational instabilities leading to a divergence of solutions. There are several empirical methods available to limit the appearance of instabilities by averaging dynamic coefficients in homogeneous directions or clipping negative model coefficient values. However, such flow-dependent solutions are not applicable in general, and they may lead to other problems, like the inability to correctly account for backscatter.⁴ To overcome these problems, many modified dynamic methods have been developed, see, e.g., reference² and other references therein. The issue that remains to be tackled is the calculation of dynamic LES coefficients by general dynamic methods in a manner that suppresses the appearance of numerical instabilities.
- P3: Consistency of hybrid RANS-LES: The computational cost of simulations is a prim concern in the design of LES equations. In particular, for wall-bounded flows the LES cost are comparable to direct numerical simulation (DNS) cost because of the need to accurately simulate the very small-scale near-wall motions. Thus, the application of LES to wall-bounded flows is still intractable for most flows at high Reynolds

*Associate Professor, Department of Mathematics, 1000 E. University Avenue, Laramie WY 82071, Email: heinz@uwyo.edu, Senior Member AIAA.

numbers. A way to overcome this cost issue is to combine LES equations with Reynolds-averaged Navier-Stokes (RANS) equations, which are used to simulate near-wall motions. RANS equations have the same structure as LES equations. They may be seen as very coarse LES equations⁵ such that their solution is much cheaper than the solution of LES equations. A variety of ideas for combining LES and RANS equations have been presented over the last fifteen years.⁶⁻⁹ However, currently there is no agreement about an optimal way to combine LES and RANS equations. The key problem here is to decipher how LES equations can be consistently combined with RANS equations.

The large number of available non-dynamic, dynamic, and hybrid LES methods leads to the question of how we can find out the best solutions to the problems P1, P2, and P3. This question can be addressed by comparisons with DNS and experimental results, but this approach can only give partial answers: it is impossible to compare a large number of LES methods, DNS comparisons are only feasible for relatively small Reynolds numbers, and experiments usually provide rather limited information. A different approach is to develop first a theoretically optimal model and to ask then whether this model is an optimal model, which requires to show that the model is a theoretically optimal model and there is no comparable alternative method which performs better in simulations. This approach will be applied here: we will determine the properties of a theoretically optimal model, show a systematic approach for designing theoretically optimal models, and demonstrate the accuracy and cost advantages of these models in comparison to other LES methods.

What are the properties of optimal solutions to the problems P1, P2, and P3 described above? Regarding the problem P1, a theoretically optimal model will be a model that has the following property

OM1: The model is realizable and systematically derived.

Realizability was proven to represent a valuable guiding principle for turbulence modeling.^{1,4} The constraint that the model is systematically derived is relevant to the understanding of the range of applicability of simulation methods. The addition of a dynamic method does not add much to the computational cost, but it reduces the need for empirical model modifications to account, for example, for wall effects. In addition to the property OM1, a theoretically optimal dynamic LES model has the following characteristic properties:

OM2a: The dynamic method is not an *ad hoc* procedure but implied by proven turbulence properties.

OM2b: The dynamic method provides local model parameters that may be negative.

OM2c: The dynamic method enables computationally stable simulations without using *ad hoc* assumptions.

Property OM2a extends the property OM1 to the requirement that the dynamic method is also supported by a theory. Property OM2b is relevant, for example, to correctly simulate transitional flows, and to enable the simulation of backscatter. Property OM2c reflects the need to have a general methodology without empirical adjustments. The extension of a non-dynamic LES model to a hybrid RANS-LES model differs from the extension of a non-dynamic LES to a dynamic LES method by the different focus on reducing the computational cost. In addition to the property OM1, the characteristic properties of a theoretically optimal hybrid LES model are the following ones:

OM3a: The hybrid model applies one velocity model; scale information enters only via the time scale model.

OM3b: The hybrid model involves a time scale that varies continuously between the RANS and LES scale.

OM3c: The hybrid model represents a single computational approach which is computationally stable.

LES and RANS equations can be described by the same velocity model.¹⁰ To define a stress, the velocity model has to be combined with a time scale model, which provides scale information. A theoretically optimal hybrid RANS-LES model should reflect this relevant property of RANS and LES models, i.e., it has to satisfy property OM3a. The design of a hybrid RANS-LES model then requires that the transition between RANS and LES equations is controlled by the time scale model. A theoretically optimal hybrid model will involve a time scale model that continuously varies between the RANS and LES scale, which corresponds to property OM3b. Such a model enables simulations without discontinuities or jumps of mean velocities near interfaces. Theoretically, the hybrid model can be defined on the basis of different coupling approaches (e.g., a RANS simulation performed prior to a hybrid RANS-LES simulation). A theoretically optimal hybrid model has to represent a single computational approach which is computationally stable. This requirement corresponds to

the property OM3c. A combination of velocity and time scale models that has the properties OM3a, OM3b, and OM3c represents a unified RANS-LES model because it combines a velocity model with a unified time scale formulation covering both the RANS and LES scale.

Theoretical solutions for the LES problems P1, P2, and P3 were suggested by Heinz.^{4,10,11} Applications of the new dynamic and unified methods are reported so far in several publications related to channel flow simulations using a new dynamic modeling approach,^{12,13} the use of channel flow data for the evaluation of computational features of unified RANS-LES methods,^{14–16} and the application of unified RANS-LES methods for the prediction and analysis of swirling turbulent jet flows.^{17,18} The purpose of this paper is to present the potential of this approach by explaining the theoretical basis and providing an overview of relevant model features. The stochastic modeling approach and the implied dynamic and hybrid RANS-LES methods are described in Sects. II, III, and IV, respectively. The performance of the dynamic modeling approach is discussed in Sect. V, and the performance of the hybrid RANS-LES modeling approach is discussed in Sect. VI. The conclusions are summarized in Sect. VII.

II. Realizable Stress Models

To derive LES equations we define a spatial filter operation for any variable f by

$$\tilde{f}(\vec{x}, t) = \int G(\vec{r}) f(\vec{x} + \vec{r}, t) d\vec{r}. \quad (1)$$

Here, $G(\vec{r})$ is a filter function, which is assumed to be homogeneous. In the following, a box filter will be applied. For the incompressible flow considered, the filtered continuity and momentum equations read

$$\frac{\partial \tilde{U}_i}{\partial x_i} = 0, \quad \frac{\tilde{D}\tilde{U}_i}{\tilde{D}t} = -\frac{1}{\rho} \frac{\partial P}{\partial x_i} + 2\nu \frac{\partial \tilde{S}_{ik}}{\partial x_k} - \frac{\partial \tau_{ik}^d}{\partial x_k}. \quad (2)$$

Here, \tilde{U}_i refers to the filtered velocity field, $\tilde{D}/\tilde{D}t = \partial/\partial t + \tilde{U}_k \partial/\partial x_k$ denotes the filtered Lagrangian time derivative, $P = \tilde{p} + 2k/3$ is the modified filtered pressure that includes a contribution due to the SGS kinetic energy k , ρ is the constant fluid mass density, and ν is the constant kinematic viscosity. The filtered rate-of-strain tensor is defined by $\tilde{S}_{ij} = (\partial \tilde{U}_i/\partial x_j + \partial \tilde{U}_j/\partial x_i)/2$. The LES equations (2) are unclosed due to the appearance of the unknown deviatoric SGS stress τ_{ij}^d , which is defined via $\tau_{ij} = \tilde{U}_i \tilde{U}_j - \tilde{U}_i \tilde{U}_j$.

An attractive approach for closing the LES equations (2) is to use a stochastic turbulence model that determines stochastic solutions of the LES equations.^{4,5,10,19} This means, the stochastic velocity model implies the incompressibility constraint, and it exactly recovers Eq. (2) for the filtered velocity. The advantage of the stochastic model is that it also implies transport equations for all the velocity moments. In particular, it can be used to derive the following transport equation for the SGS stress τ_{ij} ,^{4,5,10,11,20}

$$\frac{\tilde{D}\tau_{ij}}{\tilde{D}t} + \frac{\partial T_{kij}}{\partial x_k} + \tau_{ik} \frac{\partial \tilde{U}_j}{\partial x_k} + \tau_{jk} \frac{\partial \tilde{U}_i}{\partial x_k} = -\frac{2}{\tau_L} \left(\tau_{ij} - \frac{2}{3} c_0 k \delta_{ij} \right). \quad (3)$$

Here, T_{kij} refers to the triple correlation tensor of SGS velocity fluctuations. Equation (3) involves two model parameters: the nondimensional parameter c_0 , and the Lagrangian time scale τ_L . The parameter c_0 is related to the Kolmogorov constant C_0 by $c_0 = C_0/[C_0 + 2/3]$. An analysis reveals that $c_0 = 19/27 \approx 0.7$.^{5,10,11} An analysis of the τ_L scaling shows that $\tau_L = \ell_* \Delta k^{-1/2}$. Here, Δ denotes the filter width and the model parameter ℓ_* has a standard value $\ell_* = 1/3$.¹¹

The solution of the SGS stress equation (3) is computationally relatively expensive. A way to reduce the computational cost is to use the stress equation (3) for the derivation of algebraic stress models. The quadratic stress model obtained in this way reads¹¹

$$\tau_{ij} = \frac{2}{3} k \delta_{ij} - 2\nu_t \tilde{S}_{ij} - C_n \Delta^2 \left[\tilde{S}_{ik} \tilde{\Omega}_{kj} + \tilde{S}_{jk} \tilde{\Omega}_{ki} - 2\tilde{S}_{ik} \tilde{S}_{kj} + \frac{2}{3} \tilde{S}_{nk} \tilde{S}_{nk} \delta_{ij} \right]. \quad (4)$$

Here, $\tilde{\Omega}_{ij} = (\partial \tilde{U}_i/\partial x_j - \partial \tilde{U}_j/\partial x_i)/2$ refers to the rate-of-rotation tensor, and $C_n = \ell_*^2/3$. The SGS viscosity is given by the expression $\nu_t = C_k \Delta k^{1/2}$, where $C_k = \ell_*/3$. This parametrization for ν_t was used in several applications.^{1,21} The quadratic stress model (4) can be reduced to a linear stress model by setting $C_n = 0$.

Hence, the stress model (4) combined with an nonequilibrium model for k (i.e., a transport equation for k) can be used as an linear or quadratic nonequilibrium model.

However, this approach requires the solution of the equation for the SGS kinetic energy $k = \tau_{kk}/2$, which is implied by the stress Eq. (3). A computationally less expensive way is given by using the SGS kinetic energy equation implied by Eq. (3) to determine an equilibrium value for k . By using this value, the SGS viscosity reads $\nu_t = C_s \Delta^2 |\tilde{S}|$, where $C_s = (\ell_*/2)^{2.11}$. This model corresponds to the Smagorinsky model. The use of $\ell_* = 1/3$ recovers the standard value $C_s = (1/6)^2$ for the Smagorinsky coefficient.^{1,21} Then, the stress model considered reads

$$\tau_{ij} = \frac{2}{3} k \delta_{ij} - 2C_s \Delta^2 |\tilde{S}| \tilde{S}_{ij} - C_n \Delta^2 \left[\tilde{S}_{ik} \tilde{\Omega}_{kj} + \tilde{S}_{jk} \tilde{\Omega}_{ki} - 2\tilde{S}_{ik} \tilde{S}_{kj} + \frac{2}{3} \tilde{S}_{nk} \tilde{S}_{nk} \delta_{ij} \right]. \quad (5)$$

According to the consideration of a nonzero or zero C_n , this stress model can be used as a linear or quadratic equilibrium stress model.

III. Realizable Dynamic Stress Models

The development of dynamic LES methods, which provide local values for the model parameters C_s and C_n in Eq. (5), is based on the consideration of test-filtered LES equations. The test-filtered value of any variable f is defined by

$$\bar{f}(\vec{x}, t) = \int G_T(\vec{r}) f(\vec{x} + \vec{r}, t) d\vec{r}. \quad (6)$$

Here, $G_T(\vec{r})$ is a test filter function, which is assumed to be homogeneous. The test-filtering of the filtered continuity and momentum equations results in

$$\frac{\partial \bar{U}_i}{\partial x_i} = 0, \quad \frac{\bar{D} \bar{U}_i}{\bar{D} t} = -\frac{1}{\rho} \frac{\partial (\bar{P} + 2k^T/3)}{\partial x_i} + 2\nu \frac{\partial \bar{S}_{ik}}{\partial x_k} - \frac{\partial T_{ik}^d}{\partial x_k}. \quad (7)$$

We used here $\bar{D}/\bar{D}t = \partial/\partial t + \bar{U}_k \partial/\partial x_k$ and $\bar{S}_{ij} = (\partial \bar{U}_i/\partial x_j + \partial \bar{U}_j/\partial x_i)/2$. The test-filtered pressure is given by \bar{P} , and $k^T = L_{nn}/2$ refers to the subtest-scale (STS) kinetic energy. The STS stress, which enters Eq. (7) via its deviatoric component, is defined by $T_{ij} = \bar{U}_i \bar{U}_j - \bar{U}_i \bar{U}_j$. The difference between T_{ij} and the test-filtered SGS stress is $L_{ij} = T_{ij} - \bar{\tau}_{ij}$. The definitions of T_{ij} and τ_{ij} reveal that the Leonard stress is defined by $L_{ij} = \bar{U}_i \bar{U}_j - \bar{U}_i \bar{U}_j$. By accounting for Germano's identity $L_{ij} = T_{ij} - \bar{\tau}_{ij}$ we can write Eq. (7) as

$$\frac{\bar{D} \bar{U}_i}{\bar{D} t} + \frac{\partial L_{ik}^d}{\partial x_k} = -\frac{1}{\rho} \frac{\partial \bar{p}}{\partial x_i} + 2\nu \frac{\partial \bar{S}_{ik}}{\partial x_k} - \frac{\partial T_{ik}^d}{\partial x_k}. \quad (8)$$

A closure of Eq. (8) can be obtained by following the approach used to close the LES equation (2). The up-scaling of the stochastic model used to close the LES equation provides another stochastic model that implies Eqs. (7). The advantage of the stochastic model considered is that it also implies a transport equation for the STS stress L_{ij} , which is given by⁴

$$\frac{\bar{D} L_{ij}}{\bar{D} t} + \frac{\partial T_{kij}^T}{\partial x_k} + L_{ik} \frac{\partial \bar{U}_j}{\partial x_k} + L_{jk} \frac{\partial \bar{U}_i}{\partial x_k} = -\frac{2}{\tau_L^T} \left(L_{ij} - \frac{2}{3} c_0 k^T \delta_{ij} \right). \quad (9)$$

Here, T_{kij}^T is the STS triple correlation tensor of velocity fluctuations. The Lagrangian time scale at the test scale is given by $\tau_L^T = \ell_*^T \Delta^T (k^T)^{-1/2}$, where Δ^T denotes the test filter width and ℓ_*^T is a test-scale model parameter. The parameter c_0 is assumed to be unaffected by the scale.⁵

In correspondence to the derivation of Eq. (5) from Eq. (3), Eq. (9) can be used for the derivation of an algebraic stress model for L_{ij} .⁴ This calculation provides

$$L_{ij} = \frac{2}{3} k^T \delta_{ij} - C_s^T M_{ij} - C_n^T N_{ij}. \quad (10)$$

Here, the matrices M_{ij} and N_{ij} are given by the expressions

$$M_{ij} = 2(\Delta^T)^2 |\bar{S}| \bar{S}_{ij}, \quad N_{ij} = (\Delta^T)^2 \left[\bar{S}_{ik} \bar{\Omega}_{kj} + \bar{S}_{jk} \bar{\Omega}_{ki} - 2\bar{S}_{ik} \bar{S}_{kj} + \frac{2}{3} \bar{S}_{nk} \bar{S}_{kn} \delta_{ij} \right]. \quad (11)$$

The model parameters are given by $C_s^T = (\ell_*^T/2)^2$ and $C_n^T = (\ell_*^T)^2/3$. In correspondence to the derivation of the algebraic stress (5) we did only consider here the equilibrium STS viscosity (the nonequilibrium models can be found elsewhere⁴). The first-order approximation for L_{ij} is obtained by setting $C_n^T = 0$ in (10).

Equation (10) for L_{ij} can be used to design dynamic SGS models. First, this requires to explain how the parameters C_s^T and C_n^T in relation (10) are related to the SGS stress parameters C_s and C_n in Eq. (5). The analysis of this question shows that the test-scale coefficients C_s^T and C_n^T represent very good estimates for C_s and C_n provided that $\Delta^T < L^T$,⁴ where L^T is the characteristic length scale of STS turbulent eddies. The latter condition will be considered to be given in the following. According to Eq. (10), the deviatoric component of L_{ij} is then given by

$$L_{ij}^d = -C_s^{NDM} M_{ij} - C_n^{NDM} N_{ij}, \quad (12)$$

where the superscript NDM refers to coefficients calculated by the nonlinear dynamic model. The use of any two values for C_s and C_n will result an error of Eq. (12), which represents five conditions for C_s and C_n . This error is given by $E_{ij} = L_{ij}^d + C_s^{NDM} M_{ij} + C_n^{NDM} N_{ij}$. The quadratic error $E_{ij}E_{ji}$ becomes minimal if C_s and C_n are calculated by the relations

$$C_s^{NDM} = \frac{r_{SN}r_{LN} - r_{LS}}{1 - r_{SN}r_{SN}} \frac{|L^d|}{|M|}, \quad C_n^{NDM} = \frac{r_{SN}r_{LS} - r_{LN}}{1 - r_{SN}r_{SN}} \frac{|L^d|}{|N|}. \quad (13)$$

Here, we used for any two symmetric matrices A and B the abbreviations $|A| = \sqrt{2A_{ij}A_{ji}}$ and

$$r_{AB} = \frac{A_{ij}B_{ji}}{\sqrt{A_{lk}A_{kl}B_{mn}B_{nm}}}. \quad (14)$$

The variable r_{AB} has the property $-1 \leq r_{AB} \leq 1$ of a correlation coefficient. The subscripts L, S, N in relations (13) refer to the use of L_{ij}^d , \tilde{S}_{ij} , and N_{ij} , respectively. The use of the relations (13) for providing the SGS stress parameters C_s and C_n in Eq. (5) represents the nonlinear dynamic model (NDM).

A linearized dynamic model can be obtained by neglecting the nonlinear N_{ij} term in Eq. (12),

$$L_{ij}^d = -C_s^{LDM} M_{ij}, \quad (15)$$

where the superscript LDM refers to coefficients calculated by the linear dynamic model (LDM). The value of C_s^{LDM} that minimizes the quadratic error $E_{ij} = L_{ij}^d + C_s^{LDM} M_{ij}$ can be obtained from the relations (13) by neglecting terms involving a nonzero N_{ij} ,

$$C_s^{LDM} = -r_{LS} \frac{|L^d|}{|M|} = -\frac{L_{ij}^d M_{ji}}{M_{kl} M_{lk}}. \quad (16)$$

Relation (16) for the coefficient of the Smagorinsky model differs from the corresponding dynamic Smagorinsky model (DSM) expression. The DSM expression was obtained by combining Germano's identity $L_{ij}^d = T_{ij}^d - \tau_{ij}^d$ with the assumption $T_{ij}^d = -C_s^{DSM} M_{ij}$ for the deviatoric STS stress, which leads to $L_{ij}^d = -C_s^{DSM} H_{ij}$ instead of $L_{ij}^d = -C_s^{LDM} M_{ij}$ applied here, where $H_{ij} = 2(\Delta^T)^2 |\tilde{S}| \tilde{S}_{ij} - 2\Delta^2 |\tilde{S}| \tilde{S}_{ij}$. The latter two relations for L_{ij}^d have different support: $L_{ij}^d = -C_s^{DSM} H_{ij}$ suggested by Germano is based on an assumption for T_{ij}^d , whereas $L_{ij}^d = -C_s^{LDM} M_{ij}$ was derived by stochastic analysis.⁴

IV. Realizable Unified Stress Models

The idea of RANS-LES combinations is to significantly reduce the cost of LES. This is very important, in particular, regarding the simulation of wall-bounded flows. A solution for a unified formulation of computational methods was presented recently on the level of stochastic models.¹⁰ The LES model considered is given by Eq. (3),

$$\frac{\tilde{D}\tilde{U}_i}{\tilde{D}t} = -\frac{1}{\rho} \frac{\partial P}{\partial x_i} + 2\nu \frac{\partial \tilde{S}_{ik}}{\partial x_k} - \frac{\partial \tau_{ik}^d}{\partial x_k}. \quad (17)$$

combined with the incompressibility constraint $\partial \tilde{U}_i / \partial x_i = 0$. According to Eq. (4), the linear stress model is given by $\tau_{ij}^d = -2\nu_t \tilde{S}_{ij}$, where $\nu_t = k\tau_L/3$ and $\tau_L = \ell_* \Delta k^{-1/2}$. The nonlinear stress model is obtained

by considering the additional terms in Eq. (4). No attempt is made to calculate the model coefficient dynamically. The method described in the following can be used in two ways by using an equilibrium value for the SGS kinetic energy k (as applied regarding the discussion of the dynamic LES approach), or by using a transport equation for k . Both these variants can be combined with the consideration of a linear or quadratic stress model. For the following discussion we use the nonequilibrium variant because this variant corresponds to the applications reported below. The SGS kinetic energy $k = \tau_{kk}/2$ is then calculated via

$$\frac{\tilde{D}k}{\tilde{D}t} = \frac{\partial}{\partial x_k} \left[(\nu + \nu_t) \frac{\partial k}{\partial x_k} \right] - \tau_{kn}^d \frac{\partial \tilde{U}_n}{\partial x_k} - \frac{2(1 - c_o)k}{\tau_L}, \quad (18)$$

which follows from Eq. (3). Here, a diffusion model is used for the triple correlation T_{knn} . An analysis of these equations shows¹⁰ that the LES equations correspond to a RANS model if the LES time scale $\tau_L = \ell_* \Delta k^{-1/2}$ is replaced by the RANS time scale $\tau_L = \ell_* \tau^{RANS}$. Here, τ^{RANS} represents the RANS dissipation time scale of turbulence, which is related to the turbulence frequency by the relation $\omega = 1/\tau^{RANS}$. The time scale τ^{RANS} can be calculated via a transport equation for ω that is designed in analogy to Eq. (18).^{15,16} The unification of RANS and LES equations can be achieved by using a transfer function that relates consistently the LES time scale $\tau_L = \ell_* \Delta k^{-1/2}$ and RANS time scale $\tau_L = \ell_* \tau^{RANS}$.¹⁰ However, theoretical analyses and applications to channel flow simulations suggest that this transfer function can be simplified to $\tau_L = \ell_* \min(\Delta k^{-1/2}, \tau^{RANS})$. In this expression, k is provided by the unified k Eq. (18). The use of this expression for τ_L in Eqs. (17)-(18) results in a unified RANS-LES model that switches consistently from LES to RANS depending on the minimum.

This approach works well in channel flow simulations,^{15,16} but its use is hampered by the following fact. The calculation of τ^{RANS} via a transport equation for ω requires the RANS kinetic energy and velocities as input for the ω equation, i.e., this approach requires a RANS simulation prior to the unified LES simulation. This problem can be solved by using the unified SGS kinetic energy and velocity gradients as input for the ω equation, which is used to obtain τ^{RANS} . Thorough analyses and applications demonstrate the efficiency and accuracy of this dynamic coupling approach,¹⁴⁻¹⁸ which was used to obtain the following results.

V. Accuracy and Cost Characteristics of Realizable Dynamic Stress Models

The realizable dynamic stress models were applied to turbulent channel flow in the following way. The domain size ($L_x * L_y * L_z$) is taken to be $(2\pi * 2 * \pi)$ according to the DNS of Moser et al.²² All simulations were performed for a friction Reynolds number $Re_\tau = u_\tau \delta / \nu = 395$. Here, $u_\tau = \sqrt{\tau_w / \rho}$ is the friction velocity, τ_w refers to the wall shear stress, and δ is the half channel width. This Reynolds number was chosen to enable efficient DNS of a flow that is not significantly affected by Reynolds number effects.

DNS and LES were performed by using the OpenFOAM CFD Toolbox.²³ The dynamic LES models have been implemented inside the OpenFOAM CFD Toolbox. The calculations have been performed by using a finite-volume based method. The convection term in the momentum equation was discretized using a second-order central difference scheme. The pressure gradient that drives the flow in the channel has been adjusted dynamically to maintain a constant mass flow rate. The PISO algorithm was used for the pressure-velocity coupling.²⁴ The resulting algebraic equation for all the flow variables except pressure has been solved iteratively using a preconditioned bi conjugate gradient method with a diagonally incomplete LU preconditioning at each time step. The Poisson equation for the pressure was solved using an algebraic multi-grid (AMG) solver. When the scaled residual became less than 10^{-6} , the algebraic equation was considered to be converged. Time marching was performed using a second-order backward difference scheme. The time step was modified dynamically to ensure a constant CFL number of 0.5. Periodic boundary conditions have been employed along the streamwise and spanwise direction for all the flow variables. Along the wall normal direction, a no slip boundary condition was employed for the velocity and a zero gradient boundary condition has been used for the pressure term. A uniformly distributed grid was used along the streamwise and spanwise directions while the grid was refined in the wall normal direction using a hyperbolic tangent function. The DNS were performed on a grid size of $384 * 256 * 256$. A much higher grid resolution was used compared to the simulations of Moser et al.²² ($256 * 193 * 192$) because the current study uses a lower-order finite difference scheme while the simulations of Moser et al. used a spectral code. Based on the recommendation of Gullbrand and Chow,²⁵ the LES were performed on a grid size of $81 * 64 * 81$. This grid size was suggested by Gullbrand and Chow²⁵ to minimize the effect of numerical errors arising from second-order schemes. The numerical grid with a filter width $\Delta = (\Delta_x \Delta_y \Delta_z)^{1/3}$ was used as LES filter.

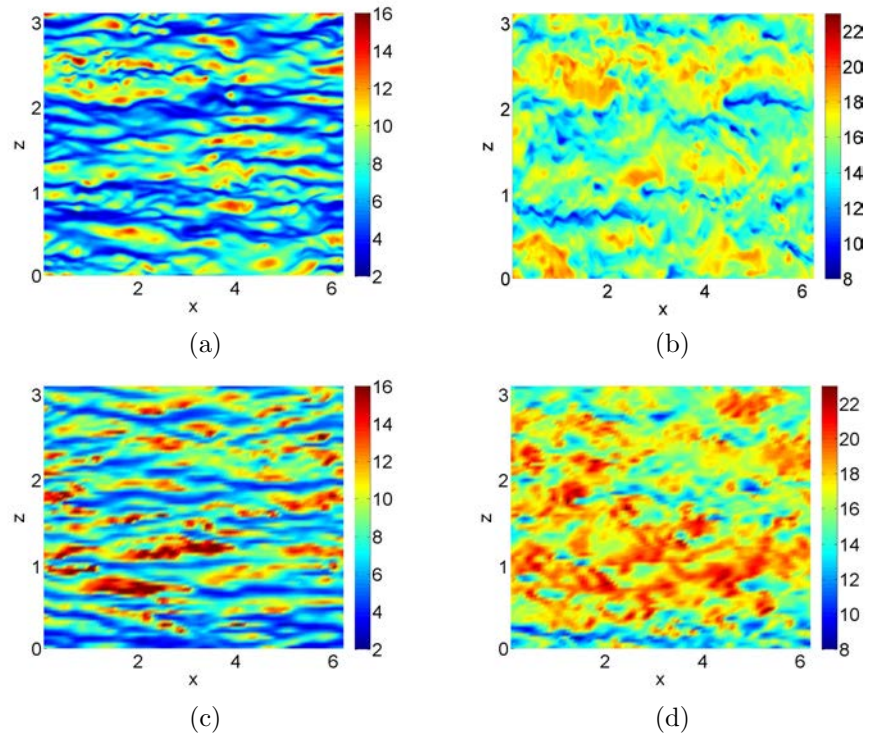


Figure 1. Instantaneous streamwise velocity contours at $y^+ = 5$ (left-hand side) and $y^+ = 50$ (right-hand side) obtained for DNS (upper row) and DNS on the $81 * 64 * 81$ grid used for performing LES (lower row).

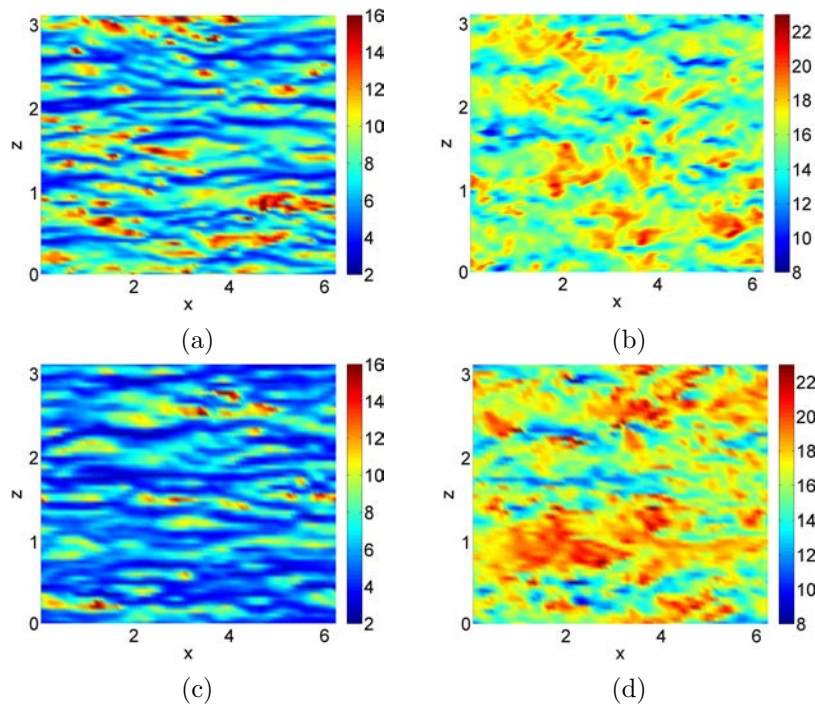


Figure 2. Instantaneous streamwise velocity contours at $y^+ = 5$ (left-hand side) and $y^+ = 50$ (right-hand side) obtained for the LDM (upper row) and DSM (lower row).

N	t^{DSM}	t^{LDM}	t^{NDM}	t^{WBDM}
64 * 64 * 64	6.48	6.26	6.76	7.23
81 * 64 * 81	11.60	11.23	12.04	12.85
122 * 64 * 122	26.88	25.63	27.21	27.83
148 * 96 * 148	62.83	60.65	64.28	65.51
223 * 96 * 223	148.35	142.50	151.70	154.08
334 * 96 * 334	333.64	329.18	364.99	371.33

Table 1. CPU time (in seconds) for performing a numerical simulation over a single time step with the dynamic models considered for the specified grid resolutions.

Compared to the non-stabilized and stabilized DSM, the advantage of the LDM is that this model enables stable simulations without clipping or averaging of the dynamic constant. To understand the effect of the stabilization procedure used for the DSM, contour plots of the instantaneous normalized streamwise velocity $U^+ = U_1/u_\tau$ obtained for the stabilized DSM and LDM will be compared with DNS data at $y^+ = 5$ and $y^+ = 50$, respectively. The comparison at $y^+ = 5$ is helpful for the evaluation of the performance of dynamic models in the near-wall region, where all the turbulence is generated. The value $y^+ = 50$ corresponds to the location of the first grid point above the wall for the case that high Reynolds number LES combined with wall-functions is performed on coarse grids (such simulations are used for LES studies of the atmospheric boundary layer). Instantaneous streamwise velocity plots obtained by using the nonlinear NDM are not shown because these plots are very similar to the LDM plots. The DNS results at $y^+ = 5$ presented in Fig. 1a show long elongated structures. These streaks agree with the structures observed in previous DNS simulations of turbulent channel flow.²⁶ At $y^+ = 50$ the length of the streaks is reduced and the organized streaky pattern seen for $y^+ = 5$ disappeared. Instead, Fig. 1b indicates the existence of three-dimensional turbulence structures covering a range of scales.²⁷ To see the relevance of SGS stress modeling, the DNS results are compared in Figs. 1c-d with results of simulations that do not apply a SGS stress model, which means DNS on the 81 * 64 * 81 grid used for performing LES. It may be seen that the neglect of the SGS stress model implies a significant overprediction of instantaneous streamwise velocities. The comparison of Fig. 1b and Fig. 1d shows that turbulence structures are merged to larger-scale structures if no SGS stress model is applied. Therefore, the neglect of a SGS stress model results in significant shortcomings regarding the representation of small-scale turbulence dynamics. The LDM results shown in Figs. 2a-b agree very well with the DNS results for both $y^+ = 5$ and $y^+ = 50$. For $y^+ = 5$ we observe elongated streaks, and the same three-dimensional turbulence structures as seen in DNS are visible for $y^+ = 50$. Compared to the DNS, the LDM results reveal a minor overprediction of the streamwise velocity. The DSM results shown in Figs. 2c-d for $y^+ = 5$ and $y^+ = 50$ differ from the DNS results. For $y^+ = 5$, Fig. 2c does not show clearly visible streaky structures, and the streamwise velocity is underpredicted. For $y^+ = 50$, Fig. 1d reveals a significant overprediction of instantaneous streamwise velocities. The turbulence structures are smeared out and merged to large-scale structures, this means the small-scale structure of turbulence is not well represented. The reason for these shortcomings of the DSM is given by the stabilization procedure applied: the averaging and clipping involved does not enable the simulation of backscatter. Therefore, the use of the LDM is definitely a better choice than the application of the DSM. The LDM involves backscatter which enables an accurate representation of small-scale turbulence, and it is capable of correctly representing the typical streaky structures seen in the near-wall region of wall-bounded flows.

Finally, the computational efficiency of different dynamic models will be quantified by considering four dynamic models: the equilibrium linear dynamic model (LDM), the equilibrium nonlinear dynamic model (NDM), the stabilized Dynamic Smagorinsky model (DSM), and the Wang-Bergstrom dynamic model (WBDM).²⁸ To enable stable simulations with the DSM, the dynamic coefficient C_s^{DSM} was locally averaged along the cell faces and numerically clipped, this means C_s^{DSM} was set to zero when it became negative to avoid numerical instabilities. This analysis was performed by using six grids for $Re_\tau = 395$: see Table I. The simulations were performed on a single-core of an AMD 2.3 GHz Opteron Processor 6134 as a dedicated process using the torque queuing system. The time step, which was chosen on the basis of the finest grid resolution, was kept constant during all simulations. The CPU time t (in seconds) for a single time step was calculated by dividing the computational time required to perform 500 time steps by 500. The values of t for the different grid resolutions are shown in Table 1. It can be seen that the LDM requires the

minimum amount of CPU time per time step followed by the DSM, NDM, and WBDM, respectively. The computational cost of the DSM are higher than the LDM cost due to the need for performing averaging, clipping and also filtering of an additional term during the calculation of the dynamic constant.¹³ The increase of the computational time for the nonlinear models arises from the need to involve the nonlinear terms and to calculate additional dynamic constants. The NDM calculations are faster than the WBDM calculations because only a 2×2 matrix needs to be inverted to calculate C_s^{NDM} and C_n^{NDM} , whereas a 3×3 matrix inversion is needed for the calculation of the dynamic constants of the WBDM. The following approach is used to quantify the computational time required for the use of the different models. An analysis of the Table I data provides support for the use of the relation

$$\frac{t}{t_0} = a \left(\frac{N}{N_0} \right)^b, \quad (19)$$

which relates the computational time t for performing a numerical simulation over a single time step to the number N of grid points applied. The introduction of the reference values $N_0 = 10^5$ and $t_0 = 2.45$ s here is helpful to simplify the model comparison ($t_0 = 2.45$ s implies $a = 1$ for the LDM). It turns out that the cost of all dynamic models considered are characterized by the same value $b = 1.05$. For each data point, the a values for the different dynamic models can be obtained by using Eq. (19). For each dynamic model, constant values of a can be calculated by taking the average over the a data obtained for each data point, where the first and last data points are not included. This leads to $a = (1.000, 1.043, 1.068, 1.101)$ for the LDM, DSM, NDM, and WBDM, respectively. The validity of using Eq. (19) in conjunction with these a values and $b = 1.05$ is confirmed in terms of Fig. 3, which shows a very good agreement between the measured cost data and the model (19). Note that the DSM, NDM, and WBDM curves are shifted upwards by (0.5, 1.0, 1.5), respectively, to improve the visibility of the comparison between measured and modeled cost data. The values $a = (1.000, 1.043, 1.068, 1.101)$ obtained for the LDM, DSM, NDM, and WBDM quantify the computational cost advantage of the LDM compared to the DSM, and the NDM compared to the WBDM. By using standard scalings for the number of grid points N required to compute a flow at a certain Reynolds number Re ,¹ Eq. (19) can be used for representing t in dependence on Re .

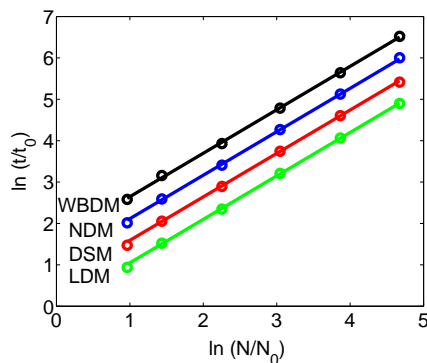


Figure 3. CPU time (in seconds) for performing a single time step of numerical simulation using the dynamic models considered for various grid resolutions. The data points are represented by circles and the fits are represented by solid lines. The DSM, NDM, and WBDM curves are shifted upwards by (0.5, 1.0, 1.5), respectively, to improve the visibility of the comparison between measured and modeled cost data.

VI. Accuracy and Cost Characteristics of Realizable Unified Stress Models

The accuracy of the unified RANS-LES model is illustrated by turbulent swirling jet flow simulations; see the illustration in Fig. 4. In a previous study we analyzed such jet flows at a Reynolds number $Re = 10^5$ for swirl numbers ranging from zero to one by using a segregated RANS-LES model.²⁹ There is convincing evidence obtained by experimental studies that vortex breakdown is found for the jet flow considered for swirl numbers $S \geq 0.6$.^{30–37} However, our simulations performed by using a segregated RANS-LES model did only show vortex breakdown for swirl numbers $S > 1$. To test the performance of the unified RANS-LES model we simulated the swirling turbulent jet flows at several swirl numbers by using a segregated RANS-LES model and the unified RANS-LES model. In particular, we used the linear nonequilibrium stress

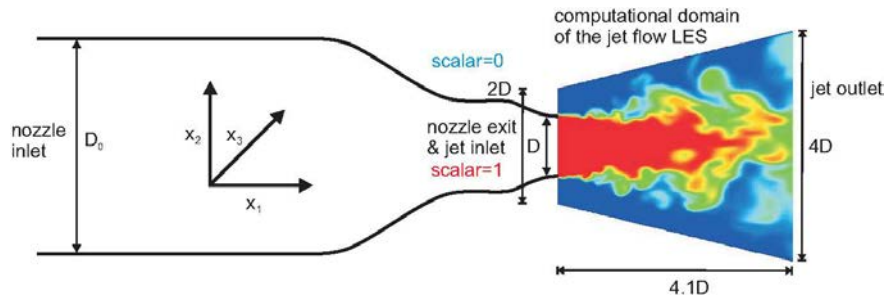


Figure 4. Results of swirl flow LES: the nozzle and jet domain are shown.

model and the omega model of Bredberg, Peng, and Davidson³⁸ for providing the RANS timecale τ^{RANS} . The nozzle region was calculated as a RANS region and the jet region was calculated as a LES region. All the simulations were performed by using the OpenFOAM CFD Toolbox. It is worth noting that the segregated RANS-LES simulations differed by our previous RANS-LES simulations²⁹ by the use of another RANS model (the omega model of Bredberg, Peng, and Davidson instead of the shear stress transport (SST) $k - \omega$ model) and another solver (OpenFOAM instead of FLUENT). Experimental data were used for the validation of simulations of the non-swirling ($S = 0$) case and a mild swirl ($S = 0.23$) case. Figure 5 shows the significant difference between the unified simulation and the segregated RANS-LES simulation. In consistency with experimental observations,^{30–37} the unified model predicts vortex breakdown, whereas the segregated RANS-LES method does not. Details of these studies can be found elsewhere.^{17,18}

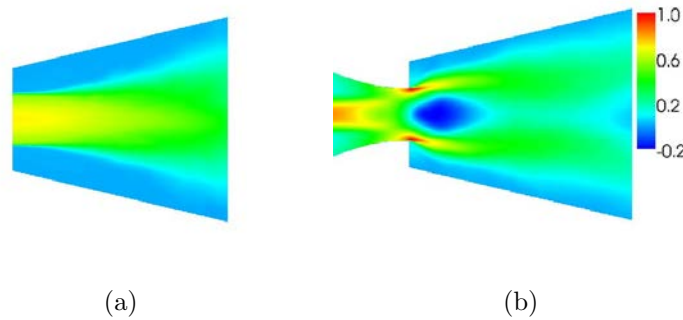


Figure 5. Results of swirl flow LES. Figure (a) shows a contour plot of the normalized mean axial velocity in the center-plane for a swirl number $S = 1$. This result was obtained by a segregated RANS-LES simulation. Figure (b) shows the corresponding result of using the unified linear LES model, which simulated the nozzle and jet flow consistently.¹⁸

The unified model does not only provide better predictions than LES, but it reduces the computational cost significantly. As shown with regard to turbulent channel flow simulations,¹⁶ the number of grid points required to perform unified RANS-LES simulations is given by

$$N = e^{13.36R_k - 10.76} Re^{2.53 - 2.29R_k}. \quad (20)$$

Here, Re refers to the Reynolds number. $R_K = k/(k + k_{res})$ is the percentage of modeled energy taken at the channel centerline and averaged over homogeneous directions. k_{res} refers to the resolved turbulent kinetic energy. To perform LES one usually applies $R_K = 0.2$, whereas the application of the unified RANS-LES model does only require $R_K = 0.4$. Hence, the use of the unified RANS-LES model reduces the cost of pure LES by a factor

$$\frac{N_{LES}}{N_{Unified}} = (e^{-13.36} Re^{2.29})^{0.2} = 0.07 Re^{0.46}. \quad (21)$$

The gain at higher Reynolds numbers can be demonstrated by the following example. The LES of the flow field around an actual wind turbine requires around 30 million grid points. The Reynolds numbers of the atmospheric flow around the wind turbine is about $Re \sim 10^9$. For this Reynolds number, the LES to unified

cost ratio given by Eq. (21) is 966. Therefore, unified simulations can be performed by using about 31000 grid points. Such cost reductions enable simulations of complex flows which are not feasible otherwise. The computational cost analysis presented here applies to the consideration of the linear unified RANS-LES model. However, the results obtained do also apply to the nonlinear unified model: the same grids are used and the bulk value R_k is hardly affected by the use of the nonlinear model. The difference between the linear and nonlinear unified models is that the nonlinear unified model requires a 10% higher simulation time than the linear unified model.

VII. Conclusions

The large number of available non-dynamic, dynamic, and hybrid LES methods leads to the question of how we can find out the best solutions to the problems P1, P2, and P3 described in the introduction. The approach suggested here is a two-stage process. First, models have to be identified which can be considered to represent theoretically optimal models. Second, it has to be shown that there is no comparable alternative method which performs better in simulations. Only in the latter case, the models can be considered to represent theoretically and computationally optimal models. A systematic approach to derive optimal solutions to the LES problems P1, P2, and P3 was described here on the basis of a common concept based on stochastic analysis.

Let us ask first whether the non-dynamic, dynamic, and hybrid LES methods described in Sects. II, III, and IV have the properties of theoretically optimal models. The four non-dynamic models presented in Sect. II (the linear and quadratic nonequilibrium and the linear and quadratic equilibrium stress models) are systematically derived from the underlying stochastic theory. These models are realizable in the sense that they are implied by a realizable stochastic model. Therefore, these models satisfy the property OM1. The corresponding four dynamic models described in Sect. III satisfy property OM2a because these models are implied by one underlying stochastic model for test-filtered velocities. Property OM2b is also satisfied because all these models provide local dynamic model parameters that may be negative. Currently available experience obtained by channel flow simulations shows that the four dynamic models do also satisfy property OM2c. The corresponding four unified RANS-LES models described in Sect. IV satisfy the properties OM3a and OM3b. The first part of property OM3c is also satisfied because the unified RANS-LES modeling approach used in the dynamic coupling option represents a single computational approach. Channel flow simulations and simulations of turbulent swirling jets flows do not indicate any stability problems of this unified RANS-LES approach, which means that these models satisfy property OM3c for the flows considered.

The second requirement for a theoretically and computationally optimal model is that there is no comparable alternative method which performs better in simulations. This question was addressed here by considering the accuracy and cost characteristics of dynamic LES and unified RANS-LES methods. Regarding the new dynamic LDM and NDM models, channel flow simulations show that the LDM and NDM are based on a dynamic concept that is more appropriate than Germano's concept used for deriving the DSM and WBDM.¹³ The LDM and NDM correctly account for backscatter and anisotropy, the small-scale structure of turbulence is represented like in DNS, and the new dynamic models are computationally stable without any modification. Compared to the DSM and WBDM, the LDM and NDM are computationally more efficient, respectively. Regarding the new unified RANS-LES models it was shown for swirling turbulent jet flow simulations that the linear unified nonequilibrium model is significantly more accurate than usually applied segregated RANS-LES models: in difference to segregated RANS-LES models this model correctly predicts vortex breakdown for swirl numbers $S \geq 0.6$. The cost advantage of unified RANS-LES models is significant compared to LES. With regard to channel flow simulations performed with the linear nonequilibrium RANS-LES model, the unified RANS-LES method provides a reduction of LES cost by a factor of $0.07 Re^{0.46}$, which is huge for a high Reynolds number Re .

What are the challenges related to the further development and application of the new dynamic LES and unified RANS-LES methods presented here? Regarding the proof that these methods do also represent computationally optimal models it needs evidence for the advantages of these methods for simulations of other flows than considered here. This concerns, in particular, applications under challenging conditions like coarse scale simulations of the atmospheric boundary layer and simulations of flows involving a significant amount of separation. Such studies are currently performed.^{39,40} From a theoretical point of view it is interesting to explore the advantages of combining unified RANS-LES methods with dynamic LES methods in order to minimize the influence of the RANS model applied and the choice of adjustable model parameters.

Acknowledgments

I am thankful to the Drs. H. Gopalan, M. Stöllinger, and C. Zemtsop for our common work. They performed the simulations and provided the figures shown in our cited publications and here. The author would like to acknowledge support through NASA's NRA research opportunities in aeronautics program (Grant No. NNX12AJ71A) with Dr. P. Balakumar as the technical officer.⁴⁰ Support through a gift from BP Alternative Energy North America Inc. to the UW Wind Energy Research Center (WERC) is also gratefully acknowledged. This work was partially supported by the UW Institute for Scientific Computation.

References

- ¹Pope, S. B., *Turbulent Flows*, Cambridge University Press, Cambridge, 2000.
- ²Sagaut, P., *Large Eddy Simulation for Incompressible Flows: An Introduction*, Springer-Verlag, Berlin, Heidelberg, New York, Tokyo, 2002.
- ³Germano, M., Piomelli, U., Moin, P., and Cabot, W., "A Dynamic Subgrid-Scale Eddy Viscosity Model," *Physics of Fluids A: Fluid Dynamics*, Vol. 3, No. 7, 1991, pp. 1760–1765.
- ⁴Heinz, S., "Realizability of Dynamic Subgrid-Scale Stress Models via Stochastic Analysis," *Monte Carlo Methods and Applications*, Vol. 14, No. 4, 2008, pp. 311–329.
- ⁵Heinz, S., *Statistical Mechanics of Turbulent Flows*, Springer-Verlag, Berlin, Heidelberg, New York, Tokyo, 1st ed., 2003.
- ⁶Spalart, P. R., Jou, W. H., Strelets, M., and Allmaras, S. R., "Comments on the Feasibility of LES for Wings, and on a Hybrid RANS/LES Approach," *1st AFOSR Intl. Conf. on DNS/LES*, Columbus: Greyden Press, Ruston, LA, USA, Aug. 4-8 1997, pp. 4–8.
- ⁷Speziale, C. G., "Turbulence Modeling for Time-Dependent RANS and VLES: A Review," *AIAA Journal*, Vol. 36, No. 2, 1998, pp. 173–184.
- ⁸Germano, M., "Properties of the Hybrid RANS/LES Filter," *Theoretical and Computational Fluid Dynamics*, Vol. 17, No. 4, 2004, pp. 225–231.
- ⁹Fröhlich, J. and von Terzi, D., "Hybrid LES/RANS Methods for the Simulation of Turbulent Flows," *Progress in Aerospace Sciences*, Vol. 44, No. 5, 2008, pp. 349–377.
- ¹⁰Heinz, S., "Unified Turbulence Models for LES and RANS, FDF and PDF Simulations," *Theoretical and Computational Fluid Dynamics*, Vol. 21, No. 2, 2007, pp. 99–118.
- ¹¹Heinz, S., "On Fokker–Planck Equations for Turbulent Reacting Flows. Part 2. Filter Density Function for Large Eddy Simulation," *Flow, Turbulence and Combustion*, Vol. 70, No. 1, 2003, pp. 153–181.
- ¹²Gopalan, H. and Heinz, S., "A New Realizable Subgrid-Scale Stress Model for Large Eddy Simulation of Neutral Atmospheric Boundary Layer," *49th AIAA Aerospace Sciences Meeting and Exhibit*, Orlando, FL, January 2011, AIAA Paper 11-556.
- ¹³Heinz, S. and Gopalan, H., "Realizable Versus Non-Realizable Dynamic Sub-Grid Scale Stress Models," *Physics of Fluids*, Vol. 24, No. 11, 2012, pp. 115105/1–23.
- ¹⁴Gopalan, H., Heinz, S., and Stöllinger, M., "Simulation of Turbulent Channel Flow Using a Linear and Non Linear Realizable Unified RANS-LES Model," *49th AIAA Aerospace Sciences Meeting and Exhibit*, Orlando, FL, January 2011, AIAA Paper 11-752.
- ¹⁵Heinz, S., Gopalan, H., and Stöllinger, M., "A Unified RANS-LES Model. Part 1. Computational Model Development," *Journal of Computational Physics*, Vol. 231, 2012, under review.
- ¹⁶Gopalan, H., Heinz, S., and Stöllinger, M., "A Unified RANS-LES Model. Part 2. Model Accuracy and Computational Cost," *Journal of Computational Physics*, Vol. 231, 2012, under review.
- ¹⁷Gopalan, H., Zemtsop, C., Stöllinger, M., and Heinz, S., "Investigation of Vortex Breakdown and Scalar Mixing in Swirling Turbulent Jet Flows Using Unified LESRANS Models," *49th AIAA Aerospace Sciences Meeting and Exhibit*, Orlando, FL, January 2011, AIAA Paper 11-768.
- ¹⁸Heinz, S., Zemtsop, C., Gopalan, H., and Stöllinger, M., "Unified RANS-LES Simulations of Swirling Turbulent Jet Flows," 2013, to be submitted.
- ¹⁹Givi, P., "Filtered Density Function for Subgrid Scale Modeling of Turbulent Combustion," *AIAA Journal*, Vol. 44, No. 1, 2006, pp. 16–23.
- ²⁰Heinz, S., *Mathematical Modeling*, Springer-Verlag, Heidelberg, Dordrecht, London, New York, 1st ed., 2011.
- ²¹Lilly, D. K., "The Representation of Small-scale Turbulence in Numerical Simulation of Experiments," *Proceedings of the IBM Scientific Computing Symposium on Environmental Sciences*, edited by H. H. Goldstone, IBM, Yorktown Heights, NY, 1967, pp. 195–210.
- ²²Moser, R. D., Kim, J., and Mansour, N. N., "Direct Numerical Simulation of Turbulent Channel Flow up to $Re_\tau = 590$," *Physics of Fluids*, Vol. 11, No. 4, 1999, pp. 943–945.
- ²³"OpenFOAM documentation (www.openfoam.org)," Tech. rep., 2009.
- ²⁴Issa, R. I., "Solution of the Implicitly Discretised Fluid Flow Equations by Operator-Splitting," *Journal of Computational Physics*, Vol. 62, No. 1, 1986, pp. 40–65.
- ²⁵Gullbrand, J. and Chow, F. K., "The Effect of Numerical Errors and Turbulence Models in Large-Eddy Simulations of Channel Flow, With and Without Explicit Filtering," *Journal of Fluid Mechanics*, Vol. 495, 2003, pp. 323–341.
- ²⁶Hoyas, S. and Jiménez, J., "Scaling of the Velocity Fluctuations in Turbulent Channels up to $Re_\tau = 2003$," *Physics of Fluids*, Vol. 18, No. 1, 2006, pp. 011702/1–4.

- ²⁷Anderson, W., Basu, S., and Letchford, C., "Comparison of Dynamic Subgrid-Scale Models for Simulations of Neutrally Buoyant Shear-Driven Atmospheric Boundary Layer Flows," *Environmental Fluid Mechanics*, Vol. 7, 2007, pp. 195–215.
- ²⁸Wang, B. C. and Bergstrom, D. J., "A Dynamic Nonlinear Subgrid-Scale Stress Model," *Physics of Fluids*, Vol. 17, No. 3, 2005, pp. 035109/1 – 17.
- ²⁹Zemtsop, C. P., Stoellinger, M. K., Heinz, S., and Stanescu, D., "Large Eddy Simulation of Swirling Turbulent Jet Flows in Absence of Vortex Breakdown," *AIAA Journal*, Vol. 47, No. 12, 2009, pp. 3011–3021.
- ³⁰Lilley, D. G., "Swirl Flows in Combustion: A Review," *AIAA Journal*, Vol. 15, No. 8, 1977, pp. 1063–1078.
- ³¹Syred, D. G. and Beer, J., "Combustion in Swirling Flows: A Review," *Combustion and Flame*, Vol. 23, No. 2, 1974, pp. 143–201.
- ³²Farokhi, S., Taghavi, R., and Rice, E., "Effect of Initial Swirl Distribution on the Evolution of a Turbulent Jet," *AIAA Journal*, Vol. 27, No. 6, 1989, pp. 700–706.
- ³³Gupta, A. K., Lilley, D. G., and Syred, N., *Swirl Flows*, Abacus Press, Cambridge, MA, 1984.
- ³⁴Huang, R. F. and Tsai, F. C., "Flow Field Characteristics of Swirling Double Concentric Jets," *Experimental Thermal and Fluid Science*, Vol. 25, No. 3-4, 2001, pp. 151–161.
- ³⁵Lucca-Negro, O. and O'Doherty, T., "Vortex Breakdown: A Review," *Progress of Energy Combustion Science*, Vol. 27, No. 4, 2001, pp. 431–481.
- ³⁶Kempf, A., Malalasekera, W., Ranga-Dinesh, K. K. J., and Stein, O., "Large Eddy Simulations of Swirling Non-premixed Flames With Flamelet Models: A Comparison of Numerical Methods," *Flow, Turbulence and Combustion*, Vol. 81, No. 4, 2008, pp. 523561.
- ³⁷Yang, Y. and Kær, S. K., "Comparison of Reynolds Averaged Navier-Stokes Based Simulation and Large-Eddy Simulation for One Isothermal Swirling Flow," *Journal of Thermal Science*, Vol. 21, No. 2, 2012, pp. 154–161.
- ³⁸Bredberg, J., Peng, S. H., and Davidson, L., "An Improved $k-\omega$ Turbulence Model Applied to Recirculating Flows," *International Journal of Heat and Fluid Flow*, Vol. 23, No. 6, 2002, pp. 731–743.
- ³⁹Stöllinger, M., Gopalan, H., Kazemi, E., and Heinz, S., "Atmospheric Boundary Layer Studies with Unified RANS-LES and Dynamic LES Methods," *51st AIAA Aerospace Sciences Meeting and Exhibit*, Grapevine, TX, January 2013, AIAA Paper.
- ⁴⁰Heinz, S., Sitaraman, J., and Mavriplis, D., "Turbulence Structure Preserving Unified and Dynamic Large Eddy Simulation of Separated Flows," *NASA's NRA Research Opportunities in Aeronautics Program*, Grant No. NNX12AJ71A, 2012-2015.